Searching for partial ruptures in Parkfield

A. R. Turner[1,2], J.C. Hawthorne [2], and C. Cattania[2]

[1]Institute for Geophysics, Jackson School of Geosciences, The University of Texas at Austin, Austin, TX, USA
[2]Department of Earth Sciences, University of Oxford, Oxford, UK
[3]Department of Geophysics, Stanford University, Stanford, CA, USA

Key Points:

- We search for partial ruptures of repeating earthquakes in Parkfield, California.
- We find partial ruptures, which suggests repeating earthquake asperities are many times larger than the nucleation radius.
- Including partial ruptures in the slip budget does not account for the repeaters' surprisingly long recurrence intervals.

Corresponding author: A.R. Turner, `alice.turner@jsg.utexas.edu`

Abstract

Repeating earthquakes repeatedly rupture the same fault asperities, which are likely loaded to failure by surrounding aseismic slip. However, repeaters occur less often than would be expected if these earthquakes accommodate all of the long-term slip on the asperities. Here we assess a possible explanation for this slip discrepancy: partial ruptures. On asperities that are much larger than the nucleation radius, a fraction of the slip could be accommodated by smaller ruptures on the same asperities. We search for partial ruptures of repeating earthquakes in Parkfield using the Northern California earthquakes catalogue. We find 3991 individual repeaters which have 4468 partial ruptures. The presence of partial ruptures suggests that asperities of repeating earthquakes are much larger than the nucleation radius. However, we find that partial ruptures could accommodate only around 25% of the slip on repeating earthquake patches. A 25% increase in the slip budget can explain only a small portion of the long recurrence intervals of repeating earthquakes.

Plain Language Summary

Repeating earthquakes happen on the same fault patch over and over again. They are thought to happen on locked patches surrounded by a slowly moving section of the fault. This slow-moving fault loads the patch to failure. However, the observed slip on the repeating earthquake patches does not match the long-term slip on the surrounding fault. This slip deficit means the time between earthquakes is longer than expected. We explore the possibility that some of the slip deficit is explained by slip happening in smaller earthquakes ("partial ruptures") in between the time of the larger magnitude repeating earthquakes. We search for partial ruptures in Parkfield, California using the Northern California earthquakes catalogue, which contains many well-located repeating earthquake sequences. We find that partial ruptures could accommodate up to 25% of the slip on repeating earthquake patches, but this is still not enough slip to explain why small repeating earthquakes occur about 5 times less often than one would expect.

1 Introduction

1.1 Long recurrence intervals of repeating earthquakes

Repeating earthquakes rupture the same asperity of a fault time and time again, with surprisingly regular recurrence intervals. These earthquakes are identified by their co-located rupture asperities, equal magnitudes, and waveform similarity (Uchida & Bürgmann, 2019; Gao et al., 2021; Waldhauser & Schaff, 2021). At first glance, repeating earthquakes seem to be an simple phenomenon; these earthquakes represent locked asperities on a fault, which are loaded to failure by the surrounding fault creep (Beeler et al., 2001). In this simple framework, the time between repeating events also seems intuitive; if the asperity is locked between earthquakes, the slip in each earthquake (S) should match the slip rate (V_{creep}) in the creeping area surrounding the repeater asperity. If the average time between repeating earthquakes is T_r, the slip per repeater should be $S = V_{creep}T_r$.

To relate the recurrence interval T_r to the moment M_0 of an earthquake, we note that the seismic slip scales with the cube root of the seismic moment:

$$S = \frac{M_0^{\frac{1}{3}}\Delta\sigma}{c\mu},\tag{1}$$

where M_0 is the seismic moment, $\Delta\sigma$ is the stress drop, μ is the shear modulus and c is a geometric constant. For a circular rupture, c = 1.81. If the slip per earthquake is equal to $V_{creep}T_r$, we find that

$$T_r = \frac{M_0^{\frac{1}{3}}\Delta\sigma}{1.81\mu V_{creep}}.\tag{2}$$

And if the stress drop is magnitude-independent, as often observed (e.g., Allmann & Shearer, 2007), this simple model of repeaters would suggest that the recurrence interval should scale as $T_r \approx M_0^{1/3}$.

However, the observed recurrence intervals of repeating earthquakes are much longer than this calculation would imply, at least given seismological estimates of the stress drop (Abercrombie, 2014; Abercrombie et al., 2020) and geodetic or geological estimates of the regional creep rate (Harris & Segall, 1987; R. M. Nadeau & Johnson, 1998). Further, repeater recurrence intervals observed globally scale with moment as $T_r \propto M_0^{0.17}$, not $M_0^{1/3}$ (R. M. Nadeau & Johnson, 1998; K. H. Chen et al., 2007). One can think of these discrepancies as a slip deficit. The observed seismic slip in the repeating earthquakes is smaller than the long-term slip on the surrounding fault.

Nevertheless, repeating earthquakes are often used as embedded creep-meters on faults.Their recurrence times are coupled with the empirical $M_0 \propto T_r^{0.17}$ scaling to estimate slip rate (e.g., Waldhauser & Schaff, 2021; Uchida & Bürgmann, 2019). However, the difference between the observed and theoretical scaling implies that we still do not fully understand the processes that create repeating earthquakes. Until we can understand the difference between the observed and theoretical scaling, repeater-based creep-meters will remain empirical, making it difficult to expand their use or understand their uncertainty.

1.2 Proposed origins of the missing slip

Researchers have proposed a range of physical models to explain the long recurrence intervals of repeating earthquakes. One set of models allows stress drop to increase as earthquakes get smaller. To match the geodetically observed slip rate in Parkfield *and* recover the $T_r \propto M_0^{0.17}$ scaling, the stress drop would have to scale as $M_0^{-1/4}$ (K. H. Chen et al., 2007). In this case, very small repeating events would require high stress drop ($\sim$ 2 GPa, Sammis & Rice, 2001). In Parkfield, repeaters are observed to have median stress drops around just 10 MPa (Abercrombie, 2014; Imanishi et al., 2004; Allmann & Shearer, 2007), though these stress drops could be underestimated if earthquakes have heterogeneous slip distributions with highly localised slip (Dreger et al., 2007; Kim et al., 2016).

A second set of models allows spatial variations in creep rate. A locally lower creep rate could be created by a boundary effect along the border between locked and creeping sections of the fault (Sammis & Rice, 2001). However, the common occurrence of repeating earthquakes is hard to reconcile with the geometrical constraints of this model – in Parkfield, 55% of earthquakes are repeating (Nadeau et al., 2004), and it is difficult to place all of these earthquakes along creeping boundaries. Instead, Williams et al. (2019) suggest that creep rate varies among the strands that compose the fault zone. In this model, repeaters have long recurrence times because the fault strands have lower slip rates than the system they compose. However, there are few observations to support this more recent model.

A final set of models allows slip on the repeater asperity between repeating earthquakes. These models suggest that much of the slip on repeater asperities accumulates aseismically or via smaller ruptures on the same asperity: via "partial ruptures" (Beeler et al., 2001; Chen & Lapusta, 2009, 2019; Cattania & Segall, 2019). As these partial ruptures take up a part of the asperity's slip budget, the recurrence interval estimate above, which includes only the slip in repeaters, will underestimate repeaters' recurrence times. Such inter-repeater slip seems plausible – we regularly see partial ruptures of locked faults around the world (e.g., Ruiz et al., 2014; Konca et al., 2008; Qiu et al., 2016; Uchida et al., 2012).

1.3 Modelled partial ruptures

In this study, we focus on this last model: where the asperity can release some moment as smaller earthquakes between the larger characteristic repeating events. In this model, the behaviour of the repeating earthquake asperity depends on the asperity radius. Specifically, behaviour depends on how big the radius is relative to the "nucleation radius" R_{nucl}: the radius of the smallest asperity that can host a seismic event (e.g., Ruina, 1983; Cattania & Segall, 2019; Chen & Lapusta, 2019, 2009).

- On repeater asperities that are only slightly larger than the nucleation radius, all ruptures on the asperity will be around the same size.
- On repeater asperities that are much larger than the nucleation radius, there are also small earthquakes that do not rupture the entire asperity. There are "partial ruptures" between complete repeater ruptures.

As such, with increasing asperity size, we expect to observe a transition from the regime where partial ruptures are not present to a regime where a large portion of the slip budget is made up of partial ruptures. The transition is estimated to occur between R $\sim$ 4.3 R_{nucl} - 6 R_{nucl} (Cattania & Segall, 2019). The presence or absence of partial ruptures could thus allow us to place a constraint on the size of repeating earthquake asperities relative to the nucleation radius.

In this study, we aim to identify and count the partial ruptures of repeating earthquakes in Parkfield, California. We will use our observations to (1) determine if slip in partial ruptures can account for the repeaters' slip deficit and explain the long recurrence intervals of repeating earthquakes and to (2) determine the size of repeater asperities relative to the nucleation radius. We will use this calibration to further tune and assess numerical models of repeating earthquakes' long recurrence intervals.

2 Finding repeaters and partial ruptures

We begin by searching for repeating earthquakes and partial ruptures in Parkfield, California. We consider two repeating earthquake catalogues. First, we use a simple approach to identify co-located earthquakes from their locations, without new waveform correlation. We take advantage of the high-quality earthquake locations already obtained in this area (Waldhauser & Schaff, 2008) and identify co-located earthquakes as earthquakes located within one rupture radius of each other. Second, we use a more sophisticated and extensive repeater catalogue created using waveform correlation by Waldhauser and Schaff (2021).

2.1 Identifying repeating earthquakes

To search for repeaters in the NCSN double-difference relocated catalogue (Waldhauser & Schaff, 2008; Schaff & Waldhauser, 2005; Waldhauser, 2013), we first select earthquakes in the 90-km-long area around Parkfield (Figure S.2), where over 50% of seismicity occurs in repeating clusters (Nadeau et al., 2004). We analyse events between 1984 and 2021, excluding ten years after the 28th September 2004 M_w 6 Parkfield earthquake; this large-magnitude event affects the moment and recurrence interval of repeating sequences (K. H. Chen et al., 2010, 2013). The analysed catalogue contains 7590 events with magnitudes between M_w -0.3 and 4.9.

We calculate each event's moment (M_0) from the catalogue magnitude (M) assuming $M_0 = 10^{1.2M+10.15}$ (Wyss et al., 2004). We then estimate the ruptures' radii. For circular ruptures, the radii R are

$$R = \left(\frac{7}{16} \frac{M_0}{\Delta\sigma} \right)^{\frac{1}{3}}. \tag{3}$$

In our primary analysis, we assume a stress drop $\Delta\sigma$ of 10 MPa, as has been inferred for events in the Parkfield region (Abercrombie, 2014; Allmann & Shearer, 2007; Imanishi & Ellsworth, 2006). We obtain similar results with a 3 MPa stress drop (section 3.4).

To search for repeating earthquakes, we cut the catalogue at the magnitude of completeness (M_w 1.1) to identify mostly complete sets of repeating earthquakes: without too many missed events. We consider each $M_w > 1.1$ earthquake in the NCSN catalogue as a potential repeater and search for co-located events: earthquakes whose catalogue locations are within one radius of this reference event horizontally as well as vertically. These co-located earthquakes are classified as potential repeaters if their magnitudes are within 0.3 magnitude units of each other. However, we remove repeater pairs separated by less than 50 days (as shown in Figure 3), as pairs with short recurrence intervals are likely to be ruptures triggered by a nearby larger mainshock, not "normal" repeating earthquakes loaded by aseismic slip. Our constraint on recurrence intervals is similar to that have been applied to repeaters by Li et al. (2007) and Bohnhoff et al. (2017).

To account for the catalogue location error, we allow an 80-m uncertainty on the horizontal location and a 97-m uncertainty on the vertical location. These uncertainties are the 90% confidence limits for relative location errors in the combined relocated and real-time catalogues. This lenient constraint will include separated earthquake pairs, providing an upper bound on the number of repeating earthquakes and partial ruptures. We additionally use the error ellipse reported in the NCSN catalogue for each event pair to provide a lower bound on the number of repeating earthquakes and partial ruptures (see section 3.4).

2.2 Identifying partial ruptures

Our search of the NCSN catalogue reveals 3991 individual repeating earthquakes: 3991 earthquakes plausibly co-located with at least one other earthquake within 0.3 magnitude units. We also have 2976 repeating earthquakes from the Waldhauser and Schaff (2021) catalogue, grouped into 612 sequences. We can now search for partial ruptures of each of these earthquakes. We again search the entire catalogue for co-located events. Here we do not truncate the catalogue at M_w 1.1. Rather, partial ruptures are events within one radius of a repeater, but with a magnitude at least 0.3 M_w units smaller.

3 Analysing repeating earthquakes and partial ruptures

Our earthquake search results in two collections of repeating earthquakes and partial ruptures. In the first collection, made by searching the relocated NCSN catalogue, we find 3991 individual repeaters. These events have 4468 partial ruptures. In the second collection, using the Waldhauser and Schaff (2021) catalogue, we find 2976 repeaters which have 2463 partial ruptures. Four examples of these repeaters and partial ruptures are illustrated in Figure 1. The repeating earthquakes are coloured in blue, and the smaller-magnitude partial ruptures are in orange. Some repeating asperities host numerous partial ruptures (e.g., panel b) while other asperities host mostly similar-magnitude events (e.g., panel c).

3.1 Moment-recurrence scaling of repeaters

We now analyse the numbers and timings of the two collections of repeating earthquakes and partial ruptures. We first analyse the repeaters' recurrence intervals. We take each identified repeater and determine the time between that event and the next repeater on its asperity. We plot this recurrence interval against the pair's average moment in Figures 2a and c for each collection of repeating earthquakes. Since there is significant scatter in the individual recurrence intervals, we also bin the pairs by moment and calculate the median recurrence interval in each moment bin. We estimate the uncertainty

of these median recurrence intervals using a bootstrapping approach. In each of 1,000 bootstrap iterations, we randomly choose 80% of the events and recompute the median recurrence interval in each bin. Finally, we perform a linear regression between the log recurrence interval and the log moment. In this regression, each recurrence interval estimate is down-weighted by the bootstrap-derived standard deviation.

In Figure 2a, the best-fitting line implies that the recurrence interval scaling for repeater pairs in the NCSN collection is $T_r \propto M_0^{0.17}$, with 95% confidence limits placing the exponent between 0.16 and 0.18 (confidence limits plotted in Figure S.3). The scaling is similar to previous estimates in the Parkfield region (R. M. Nadeau & Johnson, 1998) and elsewhere (K. H. Chen et al., 2007). In Figure 2b, the best-fitting moment-recurrence scaling for sequences from the Waldhauser and Schaff (2021) collection is $T_r \propto M_0^{0.17}$, with 95% confidence limits placing the exponent between 0.11 and 0.23.

3.2 Summed moment in repeating earthquakes and partial ruptures

Next, we analyse the moment released by repeating earthquakes and partial ruptures. For each identified repeater, we calculate the sum of the moment accommodated in similar-magnitude co-located events – the total *repeater* moment. We also calculate the sum of the moment in all co-located events, including smaller magnitude partial ruptures – the total moment. In Figure 2b and 2d we plot the total moment against the total repeater moment. The dots are coloured by the median magnitude of the co-located repeaters. Note that there is one dot per repeating earthquake (not per repeating earthquake sequence) since we analyse each repeater and its co-located events separately. Since we plot one dot per repeater but repeaters occur in sequences, we effectively analyse some earthquakes more than once, but that repetition should not influence our interpretation. As expected, the total moments are larger than the repeater moments. Including the partial rupture moment pushes the dots slightly above a one to one line in Figure 2b and 2d.

We are not interested in individual dots, but in the average moment accommodated by partial ruptures and how that moment changes with repeater magnitude. We therefore bin our observations by repeater magnitude. The repeater magnitude bins have a width of 0.43 magnitude units between M_w 1 and M_w 3.6, but varying the bin size does not strongly influence our analysis (section 3.4). In each repeater magnitude bin, we average the moments plotted in Figure 2b and 2d to obtain the mean total repeater moment and the mean total moment. The pink dots in Figure 2b and d show the mean total moment in each repeater magnitude bin plotted against the mean total repeater moment in that magnitude bin. The mean total moments are only 10 to 20% larger than the mean repeater moments in each magnitude bin; the average moment in partial ruptures seems to be small compared to the total seismic moment.

We note, however, that we are likely missing some partial rupture moment. Some small partial ruptures are likely not detected and included in the NCSN catalogue. To account for these missing earthquakes, we estimate and then correct for the NCSN catalogue's detection bias as a function of magnitude. We compute the magnitude distribution of the NCSN catalogue in the Parkfield region and note that it follows a linear Gutenberg-Richter relationship with a *b* value of 0.97 above the magnitude of completeness of M_w 1.1 (Figure S.11). We hypothesise that this distribution extends to at least $M_w = -0.5$, which is the smallest partial rupture likely to contribute a significant moment. We therefore use the observed Gutenberg-Richter distribution to compute a theoretical cumulative moment. We compute the theoretical moment between $M_w = -0.5$ and some cutoff magnitude M_{cut}, which will represent the maximum magnitude we are considering for each repeater. We also compute the observed cumulative moment: the moment in all observed earthquakes between $M_w = -0.5$ and $M_w = M_{cut}$. The ratio of the observed to the theoretical moment is a detection ratio: the fraction of the mo-

ment detected in each magnitude range. These theoretical and observed moment distributions are illustrated in Figure S.12.

We use the detection ratio as a simple correction for the moment in undetected partial ruptures. For a repeater with magnitude M_{rep}, the maximum magnitude partial rupture is (by our definition) $M_{rep}-0.3$. We therefore take the detection ratio between $M_w = -0.5$ and $M_{cut} = M_{rep}-0.3$, and we estimate the true partial rupture moment for this repeater and its co-located events by dividing the partial rupture moment by the detection ratio. This correction adds on average around $\sim 15\%$ to the moment observed in partial ruptures. We do not use this simple correction to correct the total repeater moment, as we only use repeaters above the magnitude of completeness.

Now that we have corrected all of the partial rupture moments—and thus the total moment of the events co-located with each repeater, we again average the total moments within various repeater magnitude bins. The pink triangles in Figure 2b and d show the mean corrected total moment in each repeater magnitude bin plotted against the mean total *r*epeater moment in each magnitude bin. The median moment in partial ruptures still seems to be small compared to the total seismic moment.

We plot the fraction of the moment in partial ruptures more explicitly in Figure 3. In this figure, we divide the total partial and total repeater moments by the number of repeaters in each group to obtain the mean repeater and the mean partial moments per repeater cycle. Panel a shows the partial rupture moment per cycle as a function of the mean repeater moment, and panel b shows the fraction of the moment in partial ruptures as a function of median repeater moment, with and without the correction for detection bias. The corrected moment in partial ruptures in each cycle increases from 5% to 30% between M_w 1 and M_w 2 and then decreases back toward 5 to 10%. Note, however, that we may still underestimate the moment in partial ruptures for repeaters smaller than M_w 2 because the location uncertainty is similar to the size of the asperity. The 90% error bars plotted in Figure 4 are derived from bootstrapping the earthquakes in our analysis (section 3.1); they cannot account for partial ruptures that are systematically missing because of location error. For the most robust interpretation, one may wish to focus on the results for $M_w \geq 2$ repeaters in Figure 4 and ignore the results for smaller repeaters.

3.3 Corrected moment-recurrence scaling

We were motivated to identify the moment in partial ruptures to assess whether partial ruptures could help explain the surprisingly long recurrence intervals of repeating earthquakes, as the partials could account for part of the slip budget. As such, we consider two ways to illustrate the partial ruptures' role in repeaters' slip budget: (1) by adjusting the total seismic moment and (2) by adjusting the expected slip per repeater. These equivalent representations are presented in Figure 4.

The grey circles in Figure 4a are re-plotted from Figure 2a; they show recurrence interval versus moment for individual repeating earthquakes in the NCSN collection. The larger light blue circles show averages of these values: the median recurrence intervals versus median moment for repeaters in each magnitude bin, again re-plotted from Figure 2a. However, comparing the recurrence interval to the median repeater moment ignores the moment in partial ruptures. We therefore correct these moments to include the observed partial rupture moment in each magnitude bin. We multiply the repeater moments by our inferred total-to-repeater moment ratios: by 1 plus the values plotted in Figure 3b. These corrected total moments are plotted in orange in Figure 4. The values are very similar to the uncorrected blue dots, and the best-fitting recurrence interval scaling is still $T_r \propto M_0^{0.17}$. The absolute values of the recurrence intervals, and thus the y-axis intercept, also change very little.
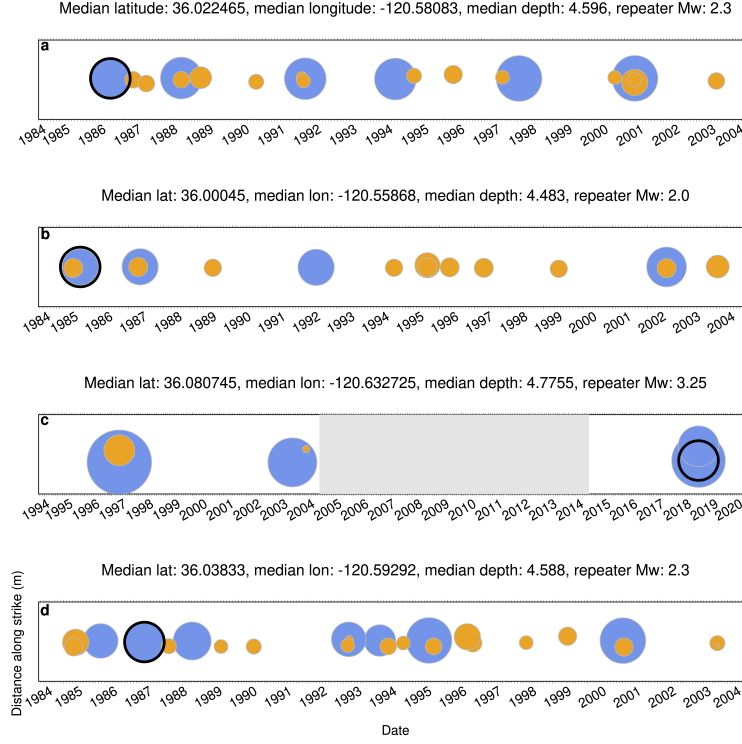
Figure 1. Examples of groups co-located earthquakes, including partial ruptures and repeating earthquakes. Repeating earthquakes are defined as similar-magnitude (within 0.3 magnitude units) co-located ruptures and are plotted in blue. Partial ruptures are smaller co-located ruptures and are plotted in orange. The event circled in black is the reference event used to identify the group of co-located events. The median latitude, longitude and magnitude of the repeating earthquakes are printed at the top of each panel. The grey box in the third panel is the ten years after the September 28th 2004 Mw 6.0 earthquake, which is excluded from this study.
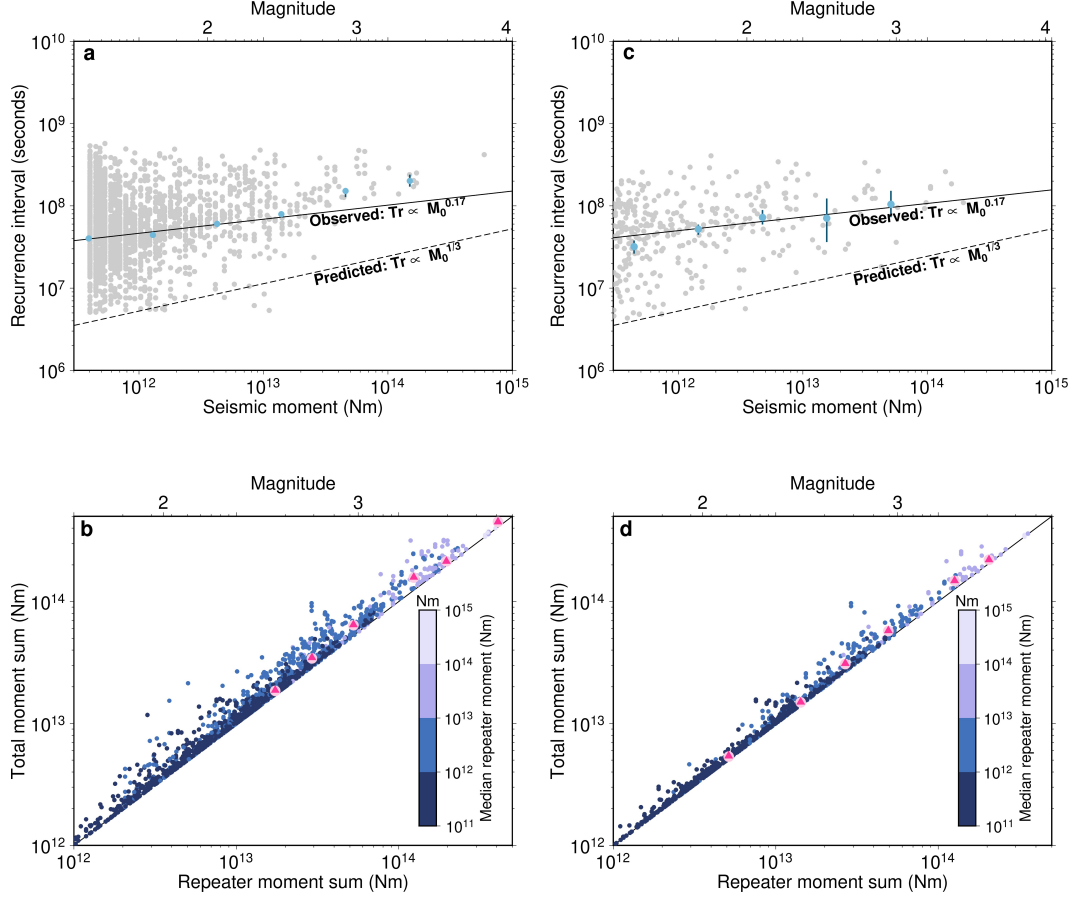
Figure 2. (a) Recurrence interval versus moment for each repeater set from the location-based NCSN repeater collection (Waldhauser, 2013). Individual values are plotted as grey circles, and medians for moment bins are plotted as blue circles. The error bars on the medians indicate 95% confidence limits, which were estimated via bootstrapping (details in the text). The best-fitting line is plotted in solid black and has a gradient of 0.17. The dashed line shows the predicted recurrence intervals assuming a stress drop of 10 MPa. (b) The total moment in repeating earthquakes (x-axis) compared to the total moment in each group of co-located events, including repeating earthquakes and partial ruptures (y-axis). Each dot is coloured by the median moment of the repeating earthquake group. Light pink dots are the means for various magnitude bins. The dark pink triangles are the binned means corrected for missing small events (see text for more details). (c) and (d) are the same as (a) and (b) using sequences from the Waldhauser and Schaff (2021) repeater collection.
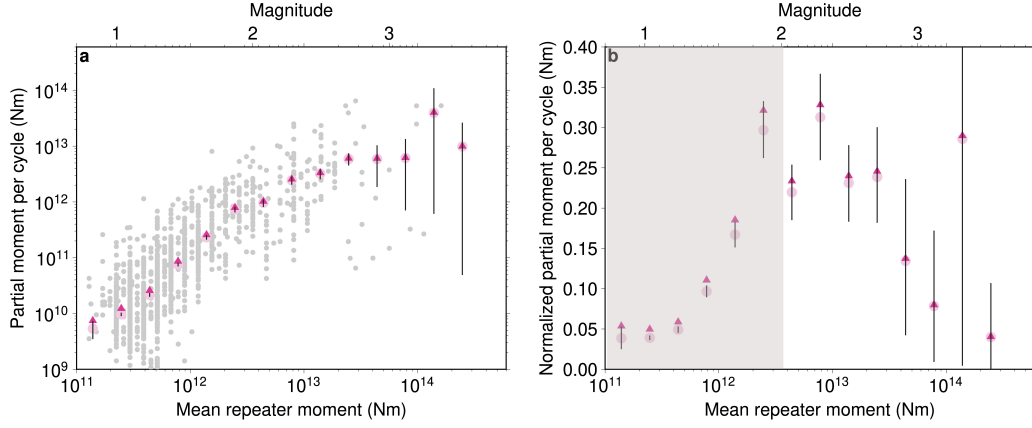
Figure 3. (a) Total moment in partial ruptures as a function of repeating earthquake moment. Both values are per cycle; the values normalised by the number of repeating earthquakes in each sequence. The dark pink triangles show the binned averages, and the black lines show the 5th and 95th percentiles of these binned medians, as derived from bootstrapping. The dark pink triangles show the binned values corrected for detection bias, as described in the text. (b) The y-axis shows the partial to repeater moment ratio: the ratio of the partial rupture moment per cycle to the mean repeater moment. The x-axis is as in panel (a): the mean repeater moment. The grey shaded region in panel (b) highlights events below M_w 2 that may have higher uncertainty due to location errors.

We also find minimal change in the scaling if we instead correct the recurrence interval for the partial rupture contribution. In Figure 4b, we convert the recurrence interval to a slip per repeating earthquake cycle. As noted in the introduction, the slip on the asperity per cycle should match the long-term slip outside the asperity so that the slip per cycle should be $S = V_{creep}T_r$, or 23 mm/yr times T_r in Parkfield (R. M. Nadeau & Johnson, 1998). The grey and blue dots in Figure 4b show the slip per cycle plotted against repeater moment, using this simple mapping from panel a. However, some of the slip per cycle is accommodated by partial ruptures. To account for the slip in partial ruptures, we divide the slip per cycle in each magnitude bin by the ratio of the total to repeater moment in that bin. As expected, the orange dots move down by 5 to 20%. The best-fitting weighted slopes increase by 23%.

Results are similar when we carry out the same analysis for the Waldhauser and Schaff (2021) repeater collection (Figure S.9).

3.4 Testing for bias in analysis

Finally, we note that in our analysis we have made a number of parameter choices: about the assumed stress drop, the local magnitude conversion, the repeater magnitude bin size, and the events' location uncertainty. To test that our observation of partial ruptures is not biased by our approach, we repeat our analysis with modifications of these parameters. First, we test whether our result changes if we modify the stress drop assumed to estimate earthquake radii (Figures S.4) or the local-to-moment magnitude conversion (Figure S.5). These modifications can change the slope of the recurrence-magnitude scaling by up to 20%, but we find that they do not significantly change the sum of the moment contained in partial ruptures.
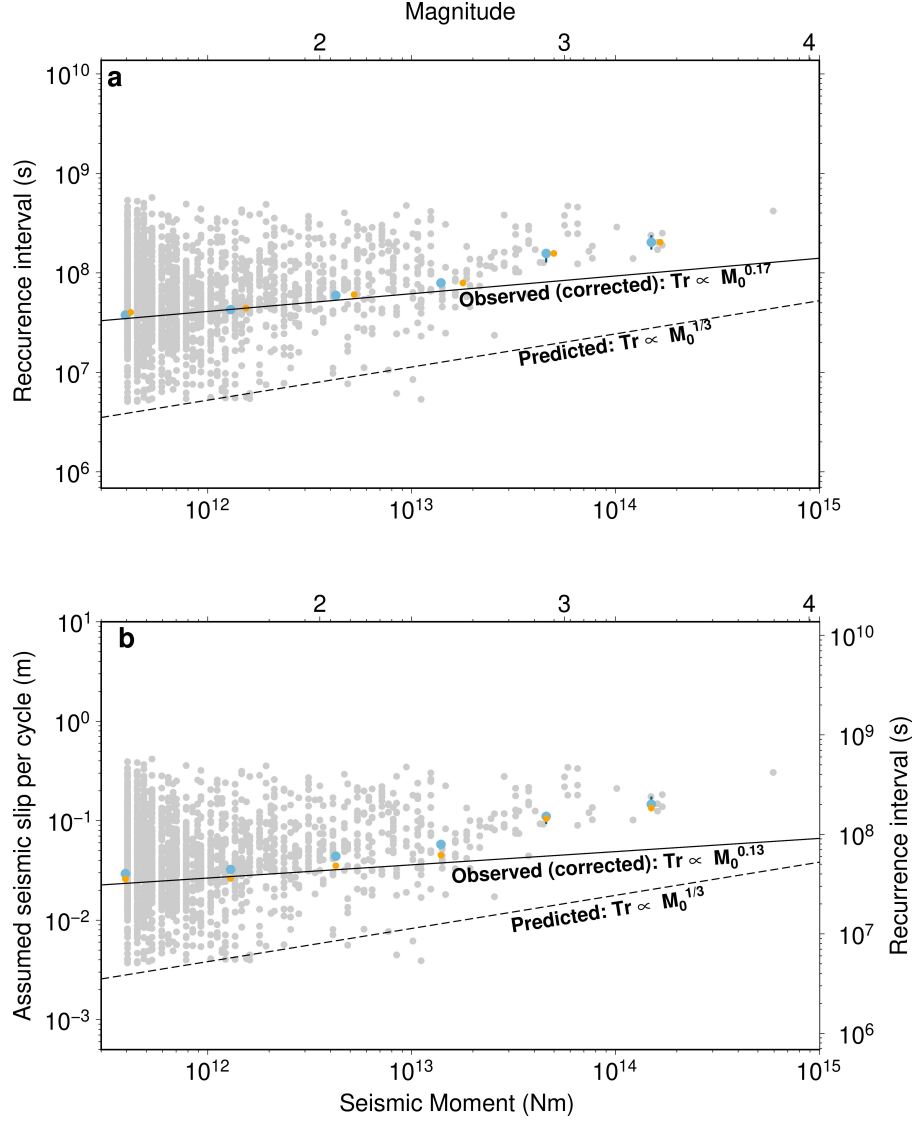
Figure 4. (a) Recurrence interval versus moment, corrected for moment in partial ruptures. The grey circles are the recurrence interval versus moment for individual repeating earthquakes in the NCSN collection, and medians for moment bins are plotted as blue circles (same as Figure 2a). We multiply the repeater moments by our inferred total-to-repeater moment ratios: by 1 plus the values plotted in Figure 3b. These corrected total moments are plotted in orange. These values are very similar to the uncorrected blue dots, and the new best-fitting recurrence interval scaling is still $T_r \propto M_0^{0.17}$. (b) Slip per repeater versus moment, corrected for slip in partial ruptures. We convert reassurance interval to slip assuming a long-term fault slip rate of 23mm/year. We divide the repeater slip by our inferred total-to-repeater moment ratios. These corrected slips are plotted in orange. The new best-fitting recurrence interval scaling is $slip \propto M_0^{0.13}$.

Next, we test the influence of the binning and down-weighting by the bootstrap-derived standard deviation on the scaling. Changing the bin size and location can influence the number of events in each bin and the standard deviation down-weighting, particularly for larger magnitude events, where bins can include as few as ~20 events. Different binning can change the slope of the scaling relationship by up to 30%, up to $T_r \propto M_0^{0.24}$, but even with uncertainty never reaches the theoretical scaling of $T_r \propto M_0^{1/3}$. And in any case, we note that this dataset is not intended to accurately determine this scaling relationship but to determine the moment accommodated in partial ruptures; that moment remains a few tens of percent or less.

We further test the influence of the events' location uncertainty with a more sophisticated approach: using the location error ellipse reported in the NCSN catalogue for each event pair instead of using cutoffs on horizontal and vertical distances separately. We compute the maximum distance between the two earthquakes that is allowed given the 95% error ellipse. Repeaters and partial ruptures are only identified if this maximum distance between a pair of events is within one rupture radius, ensuring events are co-located. This more time-consuming approach reduces the number of identified repeaters and partial ruptures by ~ 90%. However, the scaling relationship and the ratio of the moment in repeaters to the total moment in each sequence are similar (Figure S.6).

In this study, we consider two collections of repeaters and partial ruptures (Figure 4 and S.9). We find similar results when using both collections of repeaters. That does make sense, as 77% of repeaters in the NCSN collection are in the Waldhauser and Schaff (2021) collection of repeaters, and 63% of the missed events are below the magnitude of completeness (see Figure S.10). Our simple location-based criterion for locating repeating earthquakes appears to be suitable for this application in this region.

4 Discussion

4.1 Partial rupture slip budget and repeater recurrence intervals.

We were motivated to search for partial ruptures to assess whether slip in partial ruptures could account for repeaters' slip deficit and explain why repeating earthquakes occur less often than predicted. Our do observations reveal numerous partial ruptures. On typical repeater asperities, the moment in partial ruptures is 5 - 30% of the repeater moment. Those moment fractions imply that partial ruptures could accommodate up to 25% of the slip on repeating earthquake asperities. However, a 25% increase in the slip budget can explain only a factor of 1.25 increase in the recurrence intervals of repeating earthquakes. That is a small portion of the recurrence interval discrepancy that is often observed. $M_W 2$ repeaters, for instance, occur about 5 times less often than one would expect given a 10 MPa stress drop and a 23 mm/year long-term slip rate.

The partial rupture moment also appears unable to explain the scaling of repeater recurrence interval T_r with the moment. The recurrence does not change when we adjust for the partial rupture moment (Figure 4). Smaller repeating earthquakes still seem to occur particularly less often than one would expect given the long-term slip rate.

4.2 How big are repeaters relative to their nucleation radius R_{nucl}?

Partial ruptures may do more than accommodate slip. The presence or absence of partial ruptures allows us to place a constraint on the size of repeating earthquake asperities relative to the nucleation radius: the size of the smallest asperity capable of hosting seismic slip (R_{nucl}, e.g. Dieterich, 1992; Rubin & Ampuero, 2005; Chen & Lapusta, 2009; Cattania & Segall, 2019; Cattania, 2019). If repeating earthquake asperities were only slightly larger than the nucleation radius, then all ruptures on a given asperity would be around the same size, and there would be no partial ruptures.

Most repeaters in our collection do have partial ruptures. We do not observe a clear transition from no partial ruptures to partial ruptures with magnitude (Figures 3b & 4b). For instance, asperities with M_w 2 repeaters accommodate 25% of their moment in partial ruptures, and that percentage stays the same or decreases as repeater magnitude increases to M_w 3. Even asperities with M_w 1 repeaters accommodate 5% of their moment in partial ruptures, and that partial moment is likely underestimated because of earthquake location uncertainty. The consistent existence of partial ruptures implies at least that most $M_w > 2$ repeaters have $R >> R_{nucl}$.

4.3 Tuning a numerical model to match repeater recurrence?

As a final use of our partial rupture observations, we assess some models of repeating earthquakes based on crack-like ruptures (e.g., Chen & Lapusta, 2009, 2019; Cattania & Segall, 2019). These models can reproduce the observed $T_r \sim M_0^{0.17}$ recurrence interval-moment scaling. But to match observed recurrence intervals and moments, the models are tuned; modellers indirectly specify the nucleation radius, stress drop, and the long-term fault creep rate as they attempt to match the available constraints (e.g., Figure 14 of Cattania & Segall, 2019). Our observations introduce an additional constraint on the tuning: that at least $M_w > 2$ repeaters have $R >> R_{nucl}$. This constraint implies that the nucleation length R_{nucl} is a few metres or less.

This new constraint proves challenging for the models. It is not possible to tune the models to reproduce (1) a nucleation length less than a few metres, as inferred here, as well as (2) a typical stress drop around 10 MPa (Abercrombie, 2014), and (3) a long-term creep rate near Parkfield of 23 mm/yr (R. Nadeau et al., 1994). This tuning failure could indicate that a crack model coupled with rate and state friction is a poor representation of repeating earthquakes.

However, it is also possible that the models are a good representation of repeaters, and one of these observational constraints is incorrect or misinterpreted. Perhaps earthquake stress drops are actually ≥ 100 MPa, not 10 MPa, and seismic observations underestimate the stress drop because rupture models do not account for heterogeneous slip (Nadeau et al., 2004). Or perhaps the relevant long-term slip rate is much smaller, of order 4.5 cm/yr, because the fault zone is composed of several fault strands, and it is the strand's slip rate, not the regional slip rate, that drives repeaters (Chen & Lapusta, 2009; Williams et al., 2019). Alternatively, observations of partial ruptures may not accurately indicate the size of a repeater asperity relative to its nucleation size. Other fault processes such as off-fault plasticity (Mia et al., 2022) or variations in frictional properties (e.g., Uchida et al., 2007) may also encourage partial ruptures.

Given these uncertainties, it may be of interest to consider the implications of the crack model when relaxing the assumption of constant stress drop. The crack model predicts that $T_r \propto R^{1/2}$ (Cattania & Segall, 2019). For a constant stress drop, $M_0 \propto R^3$ so that $T_r \propto M_0^{1/6}$. More generally, we can write $M_0 \propto SR^2$, with S the coseismic slip, which is at most equal to the slip accumulated interseismically outside the asperity ($V_{pl}T_r$). We consider a particular scenario: where the fraction of the moment accommodated by inter-repeater slip—by aseismic slip or partial ruptures—remains constant, independent of magnitude. A constant fraction around 20% would match our observations, for instance, though it is not specifically predicted by crack-based thresholds for rupture coupled with rate and state friction given simple frictional properties Chen and Lapusta (2009); Cattania and Segall (2019); Chen and Lapusta (2019). Given such a magnitude-independent fraction, we can write $M_0 \propto T_r R^2 \propto T_r^5$. Therefore, the model predicts that if the inter-repeater moment fraction remains constant, the recurrence interval should scale with the moment as $Tr \propto M_0^{1/5}$. This scaling is close to the previously observed scaling of $Tr \propto M0^{0.17}$. Further, the stress drops should decrease with increasing repeater moment, following a $\Delta\tau \propto M_0^{-1/5}$ scaling. This magnitude scaling is small enough

to be hidden within the current uncertainty of stress drop estimates (Abercrombie et al., 2020). Perhaps it will be observed in future studies.

5 Conclusion

With this work, we sought to test the hypothesis that small repeating earthquakes have exceptionally long recurrence intervals because small earthquakes accommodate slip on the asperities between repeating earthquakes. We identify numerous partial ruptures by searching for small co-located earthquakes in Parkfield, California, using the NCSN catalogue (Waldhauser & Schaff, 2008), employing two collections of repeaters: one based on the relative locations and another created by Waldhauser and Schaff (2021). In both collections of repeaters, we find that partial ruptures accommodate only a small fraction of the moment. These fractions imply that partial ruptures could accommodate up to 25% of the slip on repeating earthquake asperities. This is not enough slip to explain why small repeating earthquakes often occur 5 times less often than one would expect.

6 Open Research

A Jupyter notebook containing a simple tutorial to identify repeating earthquakes and partial ruptures from the double-difference Earthquake Catalog for Northern California is available at $https://github.com/ARTURNER45/Partial ruptures$ (Turner, 2022).

References

Abercrombie, R. E. (2014). Stress drops of repeating earthquakes on the san andreas fault at parkfield. *Geophysical Research Letters*, *41*(24), 8784–8791.

Abercrombie, R. E., Chen, X., & Zhang, J. (2020). Repeating earthquakes with remarkably repeatable ruptures on the san andreas fault at parkfield. *Geophysical Research Letters*, *47*(23), e2020GL089820.

Allmann, B. P., & Shearer, P. M. (2007). Spatial and temporal stress drop variations in small earthquakes near parkfield, california. *Journal of Geophysical Research: Solid Earth*, *112*(B4).

Beeler, N., Lockner, D., & Hickman, S. (2001). A simple stick-slip and creep-slip model for repeating earthquakes and its implication for microearthquakes at parkfield. *Bulletin of the Seismological Society of America*, *91*(6), 1797–1804.

Bohnhoff, M., Wollin, C., Domigall, D., Küperkoch, L., Martínez-Garzón, P., Kwiatek, G., ... Malin, P. E. (2017). Repeating marmara sea earthquakes: indication for fault creep. *Geophysical Journal International*, *210*(1), 332–339.

Cattania, C. (2019). Complex earthquake sequences on simple faults. *Geophysical Research Letters*, *46*(17-18), 10384–10393.

Cattania, C., & Segall, P. (2019). Crack models of repeating earthquakes predict observed moment-recurrence scaling. *Journal of Geophysical Research: Solid Earth*, *124*(1), 476–503.

Chen, & Lapusta, N. (2009). Scaling of small repeating earthquakes explained by interaction of seismic and aseismic slip in a rate and state fault model. *Journal of Geophysical Research: Solid Earth*, *114*(B1).

Chen, & Lapusta, N. (2019). On behaviour and scaling of small repeating earthquakes in rate and state fault models. *Geophysical Journal International*, *218*(3), 2001–2018.

Chen, K. H., Bürgmann, R., & Nadeau, R. M. (2013). Do earthquakes talk to each other? triggering and interaction of repeating sequences at parkfield. *Journal of Geophysical Research: Solid Earth*, *118*(1), 165–182.

Chen, K. H., Bürgmann, R., Nadeau, R. M., Chen, T., & Lapusta, N. (2010). Postseismic variations in seismic moment and recurrence interval of repeating earthquakes. *Earth and Planetary Science Letters*, *299*(1-2), 118–125.

Chen, K. H., Nadeau, R. M., & Rau, R.-J. (2007). Towards a universal rule on the recurrence interval scaling of repeating earthquakes? *Geophysical Research Letters*, *34*(16).

Dieterich, J. H. (1992). Earthquake nucleation on faults with rate-and-state-dependent strength. *Tectonophysics*, *211*(1-4), 115–134.

Dreger, D., Nadeau, R. M., & Chung, A. (2007). Repeating earthquake finite source models: Strong asperities revealed on the san andreas fault. *Geophysical Research Letters*, *34*(23).

Gao, D., Kao, H., & Wang, B. (2021). Misconception of waveform similarity in the identification of repeating earthquakes. *Geophysical Research Letters*, *48*(13), e2021GL092815.

Harris, R. A., & Segall, P. (1987). Detection of a locked zone at depth on the parkfield, california, segment of the san andreas fault. *Journal of Geophysical Research: Solid Earth*, *92*(B8), 7945–7962.

Imanishi, K., & Ellsworth, W. L. (2006). Source scaling relationships of microearthquakes at parkfield, ca, determined using the safod pilot hole seismic array. *Washington DC American Geophysical Union Geophysical Monograph Series*, *170*, 81–90.

Imanishi, K., Ellsworth, W. L., & Prejean, S. G. (2004). Earthquake source parameters determined by the safod pilot hole seismic array. *Geophysical Research Letters*, *31*(12).

Kim, A., Dreger, D. S., Taira, T., & Nadeau, R. M. (2016). Changes in repeating earthquake slip behavior following the 2004 parkfield main shock from waveform empirical green's functions finite-source inversion. *Journal of Geophysical Research: Solid Earth*, *121*(3), 1910–1926.

Konca, A. O., Avouac, J.-P., Sladen, A., Meltzner, A. J., Sieh, K., Fang, P., ... others (2008). Partial rupture of a locked patch of the sumatra megathrust during the 2007 earthquake sequence. *Nature*, *456*(7222), 631–635.

Li, L., Chen, Q.-F., Cheng, X., & Niu, F. (2007). Spatial clustering and repeating of seismic events observed along the 1976 tangshan fault, north china. *Geophysical Research Letters*, *34*(23).

Mia, M. S., Abdelmeguid, M., & Elbanna, A. E. (2022). Spatio-temporal clustering of seismicity enabled by off-fault plasticity. *Geophysical Research Letters*, *49*(8), e2021GL097601.

Nadeau, Michelini, A., Uhrhammer, R. A., Dolenc, D., & McEvilly, T. V. (2004). Detailed kinematics, structure and recurrence of micro-seismicity in the safod target region. *Geophysical Research Letters*, *31*(12).

Nadeau, R., Antolik, M., Johnson, P., Foxall, W., & McEvilly, T. (1994). Seismological studies at parkfield iii: Microearthquake clusters in the study of fault-zone dynamics. *Bulletin of the Seismological Society of America*, *84*(2), 247–263.

Nadeau, R. M., & Johnson, L. R. (1998). Seismological studies at parkfield vi: Moment release rates and estimates of source parameters for small repeating earthquakes. *Bulletin of the Seismological Society of America*, *88*(3), 790–814.

Qiu, Q., Hill, E. M., Barbot, S., Hubbard, J., Feng, W., Lindsey, E. O., ... Tapponnier, P. (2016). The mechanism of partial rupture of a locked megathrust: The role of fault morphology. *Geology*, *44*(10), 875–878.

Rubin, A. M., & Ampuero, J.-P. (2005). Earthquake nucleation on (aging) rate and state faults. *Journal of Geophysical Research: Solid Earth*, *110*(B11).

Ruina, A. (1983). Slip instability and state variable friction laws. *Journal of Geophysical Research: Solid Earth*, *88*(B12), 10359–10370.

Ruiz, S., Metois, M., Fuenzalida, A., Ruiz, J., Leyton, F., Grandin, R., ... Campos, J. (2014). Intense foreshocks and a slow slip event preceded the 2014 iquique m w 8.1 earthquake. *Science*, *345*(6201), 1165–1169.

Sammis, C. G., & Rice, J. R. (2001). Repeating earthquakes as low-stress-drop events at a border between locked and creeping fault patches. *Bulletin of the Seismological Society of America*, *91*(3), 532–537.

Schaff, D. P., & Waldhauser, F. (2005). Waveform cross-correlation-based differential travel-time measurements at the northern california seismic network. *Bulletin of the Seismological Society of America*, *95*(6), 2446–2461.

Uchida, N., & Bürgmann, R. (2019). Repeating earthquakes. *Annual Review of Earth and Planetary Sciences*, *47*, 305–332.

Uchida, N., Matsuzawa, T., Ellsworth, W. L., Imanishi, K., Okada, T., & Hasegawa, A. (2007). Source parameters of a m4. 8 and its accompanying repeating earthquakes off kamaishi, ne japan: Implications for the hierarchical structure of asperities and earthquake cycle. *Geophysical research letters*, *34*(20).

Uchida, N., Matsuzawa, T., Ellsworth, W. L., Imanishi, K., Shimamura, K., & Hasegawa, A. (2012). Source parameters of microearthquakes on an interplate asperity off kamaishi, ne japan over two earthquake cycles. *Geophysical Journal International*, *189*(2), 999–1014.

Waldhauser, F. (2013). *Real-time double-difference earthquake locations for northern california.* Accessed.

Waldhauser, F., & Schaff, D. (2008). Large-scale cross correlation based relocation of two decades of northern california seismicity. *J. geophys. Res*, *113*, B08311.

Waldhauser, F., & Schaff, D. P. (2021). A comprehensive search for repeating earthquakes in northern california: Implications for fault creep, slip rates, slip partitioning, and transient stress. *Journal of Geophysical Research: Solid Earth*, *126*(11), e2021JB022495.

Williams, J. R., Hawthorne, J., & Lengliné, O. (2019). The long recurrence intervals of small repeating earthquakes may be due to the slow slip rates of small fault strands. *Geophysical Research Letters*, *46*(22), 12823–12832.

Wyss, M., Sammis, C. G., Nadeau, R. M., & Wiemer, S. (2004). Fractal dimension and b-value on creeping and locked patches of the san andreas fault near parkfield, california. *Bulletin of the Seismological Society of America*, *94*(2), 410–421.